nature geoscience

LETTERS

PUBLISHED ONLINE: 23 MAY 2016 | DOI: 10.1038/NGEO2719

Prebiotic chemistry and atmospheric warming of early Earth by an active young Sun

V. S. Airapetian[1]*, A. Glocer[1], G. Gronoff[2], E. Hébrard[1,3] and W. Danchi[1]

Nitrogen is a critical ingredient of complex biological molecules[1]. Molecular nitrogen, however, which was outgassed into the Earth's early atmosphere[2], is relatively chemically inert and nitrogen fixation into more chemically reactive compounds requires high temperatures. Possible mechanisms of nitrogen fixation include lightning, atmospheric shock heating by meteorites, and solar ultraviolet radiation[3,4]. Here we show that nitrogen fixation in the early terrestrial atmosphere can be explained by frequent and powerful coronal mass ejection events from the young Sun—so-called superflares. Using magnetohydrodynamic simulations constrained by Kepler Space Telescope observations, we find that successive superflare ejections produce shocks that accelerate energetic particles, which would have compressed the early Earth's magnetosphere. The resulting extended polar cap openings provide pathways for energetic particles to penetrate into the atmosphere and, according to our atmospheric chemistry simulations, initiate reactions converting molecular nitrogen, carbon dioxide and methane to the potent greenhouse gas nitrous oxide as well as hydrogen cyanide, an essential compound for life. Furthermore, the destruction of N_2, CO_2 and CH_4 suggests that these greenhouse gases cannot explain the stability of liquid water on the early Earth. Instead, we propose that the efficient formation of nitrous oxide could explain a warm early Earth.

Here we develop a new concept for the rise of prebiotic chemistry on early Earth that suggests abiotic nitrogen fixation mediated by the energy flux from palaeo-solar eruptive events. The flare statistics of Kepler data suggest that the frequency of occurrence of superflares with energies $>5\times10^{34}$ erg observed on G-type dwarfs follows a power-law distribution with a spectral index between $\alpha=-2.0$ and -2.3, which is comparable to those observed on active M-type red-dwarf stars and the Sun[5,6]. If the occurrence rate of superflares on young solar-like stars is ~0.1 events per day[6], then the frequency of super Carrington-type flare events with energy $\sim10^{33}$ erg on the early Sun ($\leq$0.5 Gyr) is expected to be ~250 events per day. Present data suggest that powerful solar flares (stronger than X5 type) are usually associated with fast ($\geq$1,000 km s^{-1}), wide ($\theta>100°$) coronal mass ejections (CMEs) and high-fluence solar energetic particle (SEP) events with kinetic energies up to 10^{33} ergs[7–9]. Tree ring data have recently provided evidence in favour of past superflares from the Sun[10,11]. Their energy is a factor of two to three times greater than that suggested for the famous Carrington-type CME event[12]. Recent direct measurements of surface longitudinal magnetic fields on young solar-type stars imply that our young Sun had generated at least ten times greater magnetic flux than that observed in the Sun at present[13]. The stronger magnetic flux produces frequent and energetic flares, fast and wide-coned CMEs and associated energetic SEP events with energies up to 10^{36} erg. Our calculations suggest that there is an approximately 5% probability of a CME striking the Earth[14]. In the 'perfect' magnetospheric storm, when the B_z magnetic field component of the incoming cloud is sheared with respect to the Earth's magnetic field, the frequency of CME impacts is greater than one event per day. To model a CME event and its effects on Earth's magnetosphere, we used the Space Weather Modeling Framework (SWMF) available through the Community Coordinated Modeling Center (CCMC) (see Supplementary Methods). We assumed a steady-state palaeo-solar wind at 0.7 Gyr with a mass loss rate of 1.7×10^{-12} M_{sun} yr^{-1} (M_{sun} is the solar mass) and a wind speed of 700 km s^{-1}, as obtained from the three-dimensional (3D) magnetohydrodynamic (MHD) young Sun's wind model[15], and a Carrington-type CME cloud propagating at a radial speed of 1,800 km s^{-1} with a total energy of 2×10^{33} erg (ref. 12). Figure 1 presents a 2D map of the steady-state plasma density superimposed with magnetic field lines for the magnetospheric configuration in the $Y=0$ plane corresponding to the initial 30 min of the simulations, when the Earth's magnetosphere was driven only by dynamic pressure from the palaeo-solar wind. Figure 1a shows the steady-state palaeo-solar wind compresses the Earth's magnetosphere to ~$9R_E$, where R_E is the Earth radius. Figure 1b shows the state of the magnetosphere two hours later when the CME cloud hits the Earth's magnetosphere (also see the movies in Supplementary Methods). At this time, the dynamic pressure of the solar wind and the magnetic reconnection between the southward directed magnetic field of the CME cloud and the northward directed dipole field of the Earth pushes the dayside magnetosphere earthwards, reducing the magnetopause stand-off distance from 9 to ~1.5 Earth radii. The CME drives large field-aligned current distributions and produces a significant disturbance of the magnetospheric field, shifting the boundary of the open–closed field to 36° in latitude and producing a polar cap opening to 70% of the Earth's dipole magnetic field. In the latest version, we used the dipole magnetic field of the Earth at present; however, palaeomagnetic studies of the Earth's ancient rocks suggest that the field was weaker[16]. This suggests that the fraction of the open field used in our model represents only a lower bound. Energetic particles accelerated in shocks driven by successive flare/CME events (see for example[17]) can then efficiently penetrate the early terrestrial atmosphere through the extended polar cap region.

We applied the Aeroplanet model[18] to simulate the atmospheric chemistry of the nitrogen-dominated (80% N_2, 20% CO_2 and 0.03% CH_4) primitive Earth's atmosphere[19]. The upper boundary of the atmosphere at 100 km is exposed to a steady-state XUV (X-ray and extreme UV) flux with the spectrum reconstructed for the early Sun

[1]NASA Goddard Space Flight Center, 8800 Greenbelt Rd, Greenbelt, Maryland 20771, USA. [2]Science Systems and Application, Inc. & NASA Langley Research Center, Hampton, Virginia 23681, USA. [3]NASA Postdoctoral Program, Universities Space Research Association, Columbia, Maryland 21046, USA. *e-mail: Vladimir.Airapetian@nasa.gov

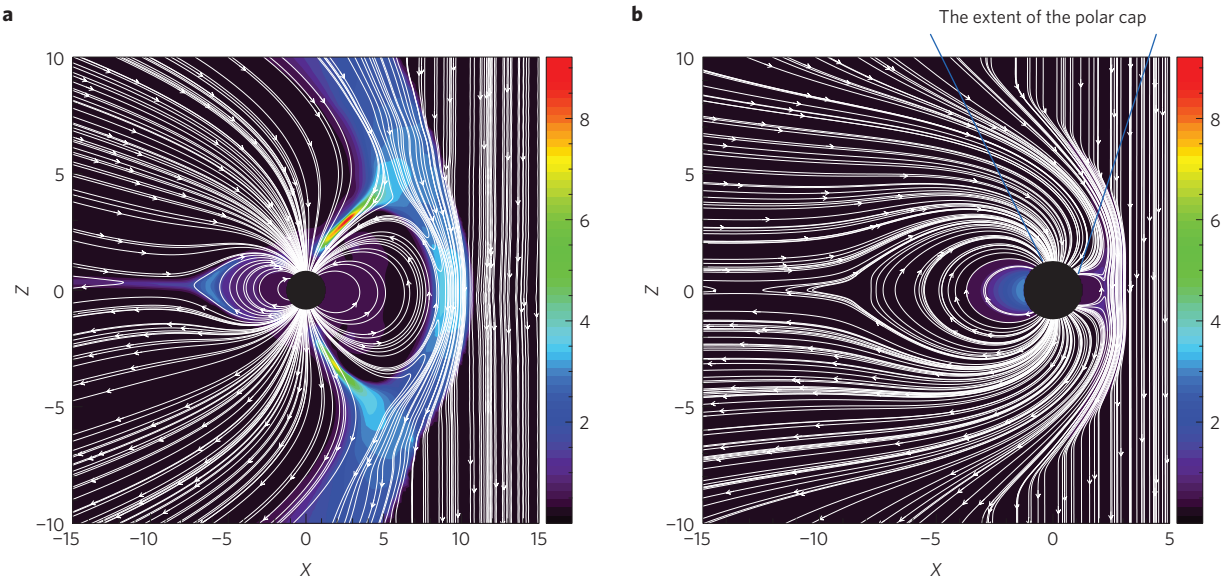

Figure 1 | Simulation of the magnetic field lines and plasma pressure in the Earth's magnetosphere due to a CME event. a, Initial state. **b**, Final state. Magnetic field lines (white) and plasma pressure in nPa (colour map)[14]. Axes represent distance from the Earth's centre in units of Earth radius.

at 0.7 Gyr (ref. 20) and to energetic protons with an energy flux of 5×10^{11} protons cm^{-2} MeV^{-1} at 0.1 MeV, with a spectral index of the energy spectrum of −2.15, representative of the 20 Jan 2005 SEP event, and an energy range within 1 GeV (ref. 21). The model calculates the photoabsorption of the EUV-XUV flux from the early Sun (see Fig. 2) as well as particle (electron and proton) fluxes to compute the corresponding fluxes at atmospheric altitudes between 200 km and the surface. These fluxes are used to calculate the photo and particle impact ionization/dissociation rates of the atmospheric species producing secondary electrons due to ionization processes. Then, using the photon flux and the photoionization–excitation–dissociation cross-sections, the model calculates the production of ionized and excited state species—and, as a result, photoelectrons. In our steady-state model of the early Earth's atmosphere, energetic precipitating protons from an SEP event impacted the middle and low atmosphere and produced ionization, dissociation, dissociative ionization, and excitation of atmospheric species—and, as a result, secondary electrons. The model includes 117 neutral chemical reactions. The destruction of N_2 into reactive nitrogen, $N(^2D)$ and $N(^4S)$, and the subsequent destruction of CO_2 and CH_4, produces NO, CO, CH and NH in the polar regions of the atmosphere, as shown in Fig. 3 (see Supplementary Methods).

Our model predicts the formation of abundant NO and NH molecules and the efficient formation of N_2O through $NO + NH \rightarrow N_2O + H$, with the major sink through the reaction $N_2O + H \rightarrow OH + N_2$ (see the pathway diagram in Fig. 3). Photolysis of N_2O through the reaction pathway $N_2O + h\nu \rightarrow N_2 + O(^1D)$, where $h\nu$ is the incident photon energy, is not an efficient loss channel for N_2O, because of the absorption of solar flux at wavelengths of less than 2,300 Å by CH_4. The atmospheric N_2O steady-state density reaches a concentration with mixing ratios of 2 and 20 ppbv at 30 km in the 1 PAL (present atmospheric level) atmosphere with 100% (solid line) and 10% (dashed line) of the maximum photochemical destruction rate, as shown in Fig. 4a. The derived value at 100% of the photodestruction rate should be considered as a lower bound, because our model does not account for a number of factors, including the eddy diffusion and convection effects, the effects of Rayleigh scattering of solar EUV radiation in the atmosphere, and the formation of hazes that significantly reduces the photodestruction rate of nitrous oxide, and therefore increases the production of N_2O. Thus, the model

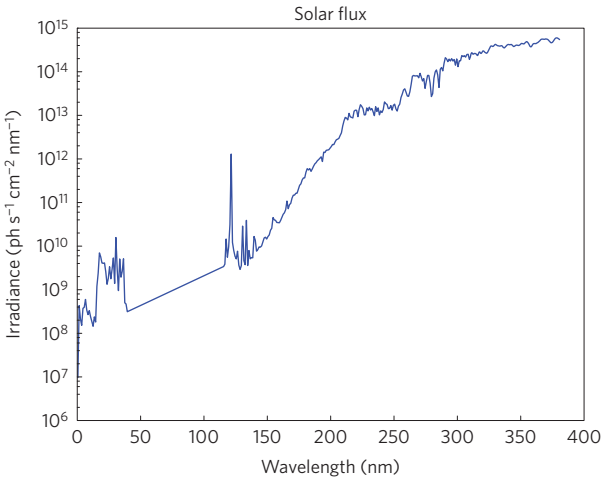

Figure 2 | Spectrum of the young Sun's XUV flux at 0.7 Gyr (ref. 20).

with 10% of the maximum photodestruction rate probably better represents the density profiles when all factors are accounted for. The steady-state density of N_2O reaches 20 to 3,000 ppbv in the 2 PAL model with 100% (solid line) and 10% (dashed line) of the maximum photochemical destruction rate, as shown in Fig. 4b. The choice of 2 PAL in Fig. 4b is consistent with compelling evidence that the atmospheric pressure of early Earth was enhanced by a factor of 2–3 (ref. 22). Another factor affecting the equilibrium mixing ratios of Fig. 4 is the representative energy of SEP events, which could be greater than that assumed in the model. Laboratory experiments have reported the production of nitrogen oxides and N_2O when a N_2–CO_2 mixture that simulates the early Earth atmosphere was exposed to lightning and coronae discharges[23]. Enhanced production of nitrous oxide in the lighting experiments is caused by energetic electrons accelerated in the discharge and by ultraviolet emission. Other evidence for the role of energetic particles in N_2O production comes from direct observations of its enhancement by 3% associated with thunderstorm events[24].

The efficient production of N_2O in our model offers a solution to warming the early Earth. The 0.7-Gyr-old Sun was 25–30% fainter

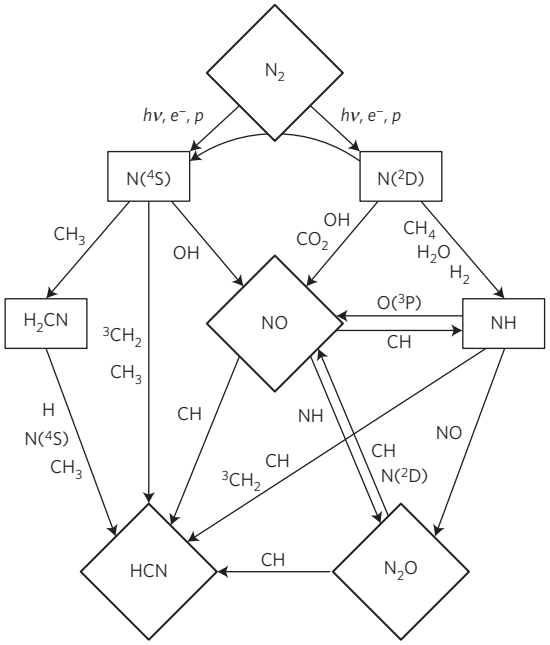

Figure 3 | The pathway diagram of abiotic production of odd nitrogen and nitrogen-bearing compounds including nitrous oxide and hydrogen cyanide due to photo and collisional dissociation and ionizations caused by XUV solar flux and SEP particle flux. Symbols e^- and *p* represent electrons and protons respectively.

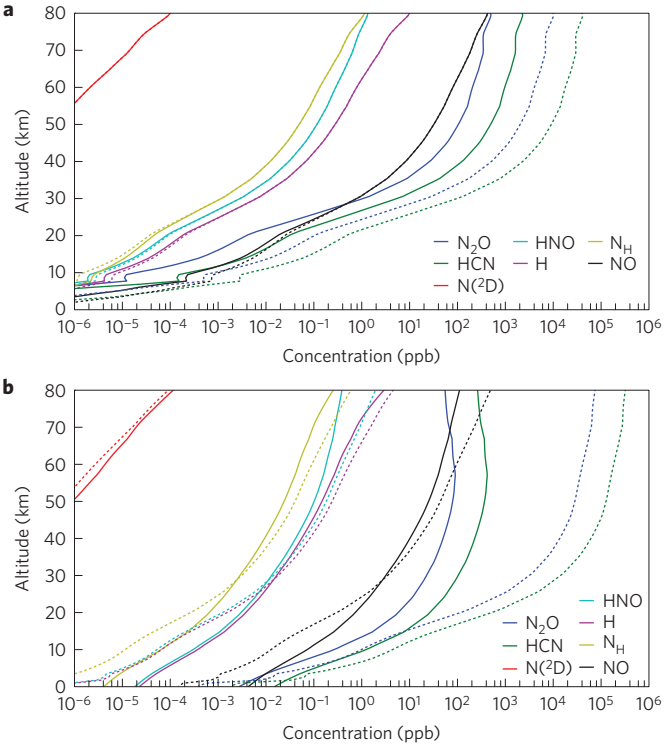

Figure 4 | Radial profiles of the steady-state mixing ratios of various species produced by an incoming flux of primary protons and secondary electrons. a,**b**, Profiles are given for 10% (dotted lines) and 100% (solid lines) of the maximum photodestruction rate at 1 PAL (**a**) and at 2 PAL (**b**).

than the present-day Sun[25], which would be insufficient to support liquid water on the early Earth, contrary to geological evidence of that time[26]. Present models of atmospheric warming offer solutions to this problem, commonly known as the faint young Sun (FYS) paradox due to a large atmospheric concentration of CO_2, H_2O, CH_4 or N_2 and H_2 (ref. 27). However, as our model implies, these molecules will be efficiently dissociated due to photo–collisional processes driven by SEPs from the young Sun, which is consistent with the recent mineralogical data[28]. Instead, the production of CH, NH and NO sets the stage for the formation of N_2O, HCN and other N-containing species in the lower parts of the atmosphere. The concentration of HCN reaches up to tens of parts per million by volume (ppmv) in the lower atmosphere. The calculated production rate of HCN in the lower atmosphere is driven mainly by the following reactions: $NO + CH \rightarrow HCN + O$, $CH_2 + N(^4S) \rightarrow HCN + H$, $CH_3 + N(^4S) \rightarrow HCN + H + H$, $CH + CN \rightarrow HCN + H$, $N_2O + CH \rightarrow HCN + NO$. Organic molecules may subsequently rain out into surface reservoirs and engage in higher-order chemistry, producing more complex organics. For example, further HCN polymerization is known to produce various amino acids, the building blocks of proteins[29]. Production of other types of soluble N-containing species (NH_3, HNO, NO) by particles may have provided a massive dose of nitrogen 'fertilizer' to early surface biology on terrestrial planets.

Thus, our concept implies that the activity of the early Sun provided a window of opportunity for prebiotic life on Earth. The proposed model also redefines the conditions of habitability, not just in terms of a 'liquid water zone', but as a biogenic zone, within which the stellar energy fluxes are high enough to ignite reactive chemistry that produces complex molecules crucial for life. As a by-product, this chemistry forms greenhouse gases that can efficiently keep the atmosphere warm enough for liquid water to exist. It will be possible to test these model predictions by observing broad and deep molecular absorption lines of N_2O at 4.5 μm and 7.9 μm and HCN absorption features at 3 and 14.3 μm of primitive terrestrial-type atmospheres around active stars through observations using the Near InfraRed Spectrograph (NIRSpec) and Mid-Infrared Instrument (MIRI) on the James Webb Space Telescope.

Methods

Methods, including statements of data availability and any associated accession codes and references, are available in the online version of this paper.

Received 14 August 2015; accepted 19 April 2016; published online 23 May 2016

References

1. Barrett, G. C. & Elmore, D. T. *Amino Acids and Peptides* (Cambridge Univ. Press, 1998).
2. Ringwood, A. E. Chemical composition of the terrestrial planets. *Geochim. Cosmochim. Acta* **30,** 41–104 (1996).
3. Summers, D. P., Basa, R. C. B., Khare, B. & Rodoni, D. Abiotic nitrogen fixation on terrestrial planets: reduction of NO to ammonia by FeS. *Astrobiology* **12,** 107–114 (2012).
4. Kasting, J. F. Bolide impacts and the oxidation state of carbon in the Earth's early atmosphere. *Orig. Life Evol. Biosph.* **20,** 199–231 (1990).
5. Maehara, H. *et al*. Superflares on solar-type stars. *Nature* **485,** 478–481 (2012).
6. Shibayama, T. *et al*. Superflares on solar-type stars observed with *Kepler*. I. Statistical properties of superflares. *Astrophys. J. Suppl. Ser.* **209,** 5 (2013).
7. Gopalswamy, N. *et al*. Properties of ground level enhancement events and the associated solar eruptions during solar cycle 23. *Space Sci. Rev.* **171,** 23–60 (2012).
8. Tsurutani, B. T., Smith, E. J., Pyle, K. R. & Simpson, J. A. Energetic protons accelerated at corotating shocks - Pioneer 10 and 11 observations from 1 to 6 AU. *J. Geophys. Res.* **87,** 7389–7404 (1982).
9. Emslie, A. G. *et al*. Global energetics of thirty-eight large solar eruptive events. *Astrophys. J.* **759,** 71 (2012).
10. Miyake, F., Nagaya, K., Masuda, K. & Nakamura, T. A signature of cosmic-ray increase in AD 774–775 from tree rings in Japan. *Nature* **486,** 240–242 (2012).
11. Miyake, F., Masuda, K. & Nakamura, T. Another rapid event in the carbon-14 content of tree rings. *Nature Commun.* **4,** 1748 (2013).

12. Tsurutani, B. T., Gonzales, W. D., Lakhina, G. S. & Alex, S. The extreme magnetic storm of 1–2 September 1859. *J. Geophys. Res.* **108,** 1268 (2003).
13. Vidotto, A. A. *et al*. Stellar magnetism: empirical trends with age and rotation. *Month. Not. R. Astron. Soc.* **441,** 2361–2374 (2014).
14. Airapetian, V., Glocer, A. & Danchi, W. in *Proc. 18th Cambridge Workshop on Cool Stars, Stellar Systems, and the Sun* (eds van Belle, G. & Harris, H.) 257–268 (2015).
15. Airapetian, V. S. & Usmanov, A. V. Reconstructing the solar wind from its early history to current epoch. *Astrophys. J.* **817,** L24–L30 (2016).
16. Tarduno, J., Blackman, E. G. & Mamajek, E. E. Detecting the oldest geodynamo and attendant shielding from the solar wind: implications for habitability. *Phys. Earth Planet. Inter.* **233,** 68–87 (2014).
17. Liu, Y. D. *et al*. Observations of an extreme storm in interplanetary space caused by successive coronal mass ejections. *Nature Commun.* **5,** 3481 (2014).
18. Gronoff, G. *et al*. The precipitation of keV energetic oxygen ions at Mars and their effects during the comet Siding Spring approach. *Geophys. Res. Lett.* **41,** 4844–4850 (2014).
19. Cnossen, I. *et al*. Habitat of early life: solar X-ray and UV radiation at Earth's surface 4–3.5 billion years ago. *J. Geophys. Res.* **112,** E02008 (2007).
20. Claire, M. W. *et al*. The evolution of solar flux from 0.1 nm to 160 μm: quantitative estimates for planetary studies. *Astrophys. J.* **757,** 95 (2012).
21. Mewaldt, R. A. Energy spectra, composition, and other properties of ground-level events during solar cycle 23. *Space Sci. Rev.* **171,** 97–120 (2012).
22. Goldblatt, C. *et al*. Nitrogen-enhanced greenhouse warming on early Earth. *Nature Geosci.* **2,** 891–896 (2009).
23. Nna-Mvondo, D., Navarro-González, R., Raulin, F. & Coll, P. Nitrogen fixation by corona discharge on the early precambrian Earth. 2005. *Orig. Life Evol. Biosph.* **35,** 401–409 (2005).
24. Brandvold, D. K., Martinez, P. & Hipsh, R. Field measurements of O_3 and N_2O produced from a corona discharge. *Atmos. Environ.* **30,** 973–976 (1996).
25. Gough, D. O. Solar interior structure and luminosity variations. *Solar Phys.* **74,** 21–34 (1981).
26. Kasting, J. F. Early Earth: faint young Sun redux. *Nature* **464,** 687–689 (2010).
27. Wordsworth, R. & Pierrehumbert, R. Hydrogen–nitrogen greenhouse warming in Earth's early atmosphere. *Science* **339,** 64–67 (2013).
28. Rosing, M. T., Bird, D. K., Sleep, N. H. & Bjerrum, C. J. No climate paradox under the faint early Sun. *Nature* **464,** 744–747 (2010).
29. Miyakawa, S., Cleaves, H. J. & Miller, S. L. The cold origin of life: B. implications based on pyrimidines and purines produced from frozen ammonium cyanide solutions. *Orig. Life Evol. Biosph.* **32,** 209–218 (2002).

Acknowledgements

This work was supported by NASA GSFC Science Task Group funds. V.S.A. performed the part of this work while staying at ELSI/Tokyo Tech. G.G. was supported by NASA Astrobiology Institute grant NNX15AE05G and by the NASA HIDEE Program, E.H. was supported by an appointment to the NASA Postdoctoral Program at NASA Goddard Space Flight Center, administered by Universities Space Research Association through a contract with NASA.

Author contributions

V.S.A. conceived and designed the numerical experiments, analysed the data, contributed materials and wrote the manuscript. A.G. and G.G. contributed to the development and execution of codes and data analysis. E.H. contributed to the chemistry model and data analysis, W.D. contributed to development of the manuscript, to data analysis and proofreading of the paper.

Additional information

Supplementary information is available in the online version of the paper. Reprints and permissions information is available online at www.nature.com/reprints. Correspondence and requests for materials should be addressed to V.S.A.

Competing financial interests

The authors declare no competing financial interests.

Methods

Description of the Space Weather Modeling Framework (SWMF). In this paper, we made use of the Space Weather Modeling Framework (SWMF), available at the Community Coordinated Modeling Center (CCMC) at NASA Goddard Space Flight Center (see http://ccmc.gsfc.nasa.gov). The main part of the SWMF consists of the single-fluid, time-dependent fully nonlinear 3D magnetohydrodynamic (MHD) code BATS-R-US (Block-Adaptive-Tree Solar-wind Roe-type Upwind Scheme)[30,31], which was developed at the University of Michigan Center of Space Environment Modeling (CSEM) and is coupled to the Rice Convection Model (RCM)[31] to model the propagation and interaction of a super-Carrington-type CME event with the magnetosphere and ionosphere of the young Earth. The MHD code calculates the dynamic response of the large-scale magnetospheric plasma to varying solar wind conditions in a self-consistent manner[30]. The dynamics of the magnetosphere is described in a Cartesian geometry by means of resistive MHD equations. The electromagnetic coupling of the magnetosphere to a conducting ionosphere is handled in a standard way[32]. Specifically, magnetospheric currents near the inner boundary of the MHD simulation are mapped to the ionosphere, where a potential solver is then used to combine these currents with a conductance map of the ionosphere (including solar and auroral contributions) to produce the electric potential in the ionosphere. This potential is then used to set the electric field and corresponding drift at the inner boundary of the magnetospheric simulations.

The MHD approximation does not provide an adequate description of the inner magnetosphere because energy-dependent particle drifts and the evolution of ring currents become important. Here we use the RCM, embedded in the MHD simulation, to model this important region[31]. The RCM code is a kinetic plasma model that couples plasma motions in the inner magnetosphere and calculates the energy-dependent particle drifts and evolution of ring currents in the inner magnetosphere. The ring current carries the most of the energy density during magnetic storms, and is essential in modelling strong storms. This coupling is crucial for a description of the effects of the solar wind on the magnetosphere, because the ionosphere provides closure of magnetospheric currents, which is needed for a realistic description of magnetospheric convection and the associated electric fields. Thus, we apply a dedicated inner magnetospheric model that is fully coupled to the MHD code for the treatment of the inner magnetosphere. We simulate the magnetospheric cavity (outer and inner magnetosphere) in a computational box defined by the following dimensions $-224R_E < x < 224R_E$, $-128R_E < y < 128R_E$, $-128R_E < z < 128R_E$, where R_E is the radius of the Earth, which is placed at the centre of the computational box. The dipole tilt is neglected in this problem. The simulations were carried out using a block-adaptive high-resolution grid with a minimum cell size of 1/16 R_E.

The inner boundary is set at 1.25 R_E with a density of 100 cm^{-3}. The velocity at the inner body is set to the $\mathbf{E} \times \mathbf{B}$ velocity, where $\mathbf{E}$ is determined from the ionospheric potential and $\mathbf{B}$ is the Earth's magnetic field. The pressure is allowed to float. The magnetic field is set in such a way that the radial component is the Earth's dipole and the tangential components are allowed to float. The simulation is initialized with a dipole everywhere in the computational domain and a low density, zero velocity, and finite pressure. The solar wind conditions are set at the upstream boundary and some period of local time stepping is used to get an initial steady-state solution. We assume the solar wind input parameters, including the three components of the interplanetary magnetic field, B_x, B_y and B_z, the plasma density, N_e, and the wind velocity, V_x, using the physical conditions associated with a Carrington-type event as discussed in refs 14,33 (see Fig. 1). The time evolution of the plasma pressure (in nPa) and current density (in $\mu A\ m^{-2}$) during the extreme CME event are presented in Supplementary Movie 1.

Description of the Aeroplanets model. We used our sophisticated Aeroplanets model with an enhanced chemistry[18] to model the response of the upper atmospheric region (up to 200 km) to the fluxes of XUV emission and SEP energetic particles from the young Sun. The model calculates the photo and collisional (due to protons) dissociation, ionization and photoexcitation processes in the Earth's atmosphere. The primary photoelectrons are then transported along a magnetic field line, and the electron impact is computed by solving the stationary kinetic Boltzmann equation. This results in the dissociation, ionization and excitation of the different atmospheric species. The Aeroplanets code incorporates 117 chemical reactions, with the rates presented in Supplementary Table 1.

Convergence to a steady-state chemical solution for the early Earth atmosphere described in the main section of the paper was reached after running the code for six months of physical time.

Code availability. The BATS-R-US code, as a part of SWMF used to generate the scenario shown in Fig. 1, can be accessed through Goddard Space Flight Center's CCMC run-on-request website at http://ccmc.gsfc.nasa.gov. We have opted not to make the computer code, Aeroplanets, associated with this paper available because we are at present in the process of adapting it for free access through the Exoplanetary part of CCMC's website.

Data availability. The authors declare that model data supporting the findings of this study are available within the article and its Supplementary Information. Other model-related data will be available on request from the authors.

References

30. Powell, K. G., Roe, P. L., Linde, T. J., Gombosi, T. I. & De Zeeuw, D. L. A solution-adaptive upwind scheme for ideal magnetohydrodynamics. *J. Comp. Phys.* **154,** 284–309 (1999).
31. de Zeeuw, D. L. *et al*. Coupling of a global MHD code and an inner magnetospheric model: initial results. *J. Geophys. Res.* **109,** A12219 (2004).
32. Ridley, A. J. *et al*. University of Michigan MHD results of the geospace global circulation model metrics challenge. *J. Geophys. Res.* **107,** 1290 (2002).
33. Ngwira, C. M., Pulkkinen, A., Kuznetsova, M. M. & Glocer, A. Modeling extreme "Carrington-type" space weather events using three-dimensional global MHD simulations. *J. Geophys. Res.* **119,** 4456–4474 (2014).